Applied Surface Science 372 (2016) 93–99

Contents lists available at ScienceDirect

Applied Surface Science

journal homepage: www.elsevier.com/locate/apsusc

Influence of Cu/Sn mixture on the shape and structure of crystallites in copper-containing films: Morphological and X-ray spectroscopy studies

ARTICLE INFO

Keywords:
Copper oxide and Cu/Sn mixed oxide crystallites
Surface morphology
Thin films
Sol-gel technique
SEM
X-ray spectroscopy

ABSTRACT

The copper-containing SiO_2CuO_x and $SiO_2(CuO_xSnO_y)$ films were deposited on to oxidized silicon substrates from the alcoholic solutions employing the sol-gel technique. The morphological and structural properties of the films were investigated by the SEM, EDX, XRD, XPS, XAS. The SEM studies have found grain shape changes from flower-like agglomerates to regular shaped inorganic ones as a result of adding the $SnCl_4$ into the sol. So, the tin adding prevents the formation of the flow-like agglomerates. In accordance with XPS data, CuO, CuO_2 and $CuSiO_3$ phases present in the both samples. Adding of the tin decreases the content of CuO_2 and increases $CuSiO_3$ on the surface and in volume of the films. The mixed-oxide crystallites are formed in SiO_2CuO_x and in $SiO_2(CuO_xSnO_y)$ grains consist of copper- oxides and SnO_2. Presence of tin oxide particles in the films decreases the response to NO_2 gas, but at the same time expands the range of detectable concentrations.

1. Introduction

In recent years, developing ways of tuning the structure of materials on specific morphologies have been one of the most important goals of materials science. One of the main problems in the synthesis of gas adsorbent and catalytically active nanocomposites is to increase and develop the surface of active sorbent center [1,2]. In metal-oxide containing nanocomposites, metal-oxide crystallites/nanoparticles often play the role of the adsorption centers and their adsorption activity depends on the size, shape, structure and the oxidation state [3–5]. The morphology and phase-structure composition of nano- microcrystals as well as composition and morphological details of matrix have great effects on electrical and adsorption properties of the resulting composites and films based on them [6–8]. The reason of this is that gas-sensing by metal-oxide semiconductors is based on the oxidation–reduction reaction of the detected gases occurring on the semiconductor surface, which leads to an abrupt change in conductance of the sensor. Besides, the influence of the matrix surface in directing the nano-unit nucleation and subsequent organization of metal oxide nanoparticals/microcrystals is observed [9]. Thus, controlled synthesis of inorganic nanostructures in terms of size and shape strongly motivated by their size and shape dependent gas adsorption and catalytically properties [10,11]. Copper oxides are capable to formation of variety nanostructures with wide range of active surface, from cubes [12], octahedrons [13] and rhombic-dodecahedrons [14] to stars [15], flower-shaped [16] etc. Furthermore, copper and tin oxides arouse a tremendous interest toward its gas sensing properties due to significant changes of the surface electrical conductivity because of chemisorption and catalytic reactions in the presence of even low concentration of CO, SO_2, NO_2, etc. [6,17,18]. Bi-component compounds often exhibits better properties (i.e., catalytic activity, electrochemical reactivity and mechanical stability) in comparison with the single ones owing to the bi-component composite integrating two types of functional materials [19]. Particular emphasis is placed on the mixed Sn-Cu alloys and SnO_x:CuO_x composites since in depends on Cu:Sn interaction allows produce materials with different surface morphology as well as crystallites structure and as consequence electrical and adsorption properties [20,21].

The next important issue is possible oxidation states for copper in the embedded microcrystals. In fact, copper forms two stable semiconducting oxides, tenorite (CuO) and cuprite (Cu_2O), and both can be prepared as embedded NPs/microcrystals in silica matrix by various chemical and physical methods [22,23]. Conversely, the formation of single-phase metallic NPs/microcrystals in silica is not straightforward and has to be pursued by a proper combination of synthesis parameters and processing conditions.

This task is complicated by the embedding into the silicon matrix bi-component compounds, like SnO_x:CuO_x. Consequently, beyond the control of copper-containing crystallites size and distribution, the tailoring of the guest copper-phase composition in the host silica matrix constitutes a major concern. Previous our works reports the changes of morphological and structural characteristics of SiO_2CuOx films in depending on different copper concentrations in the initial solution [24].

The aim of this work is to compare the morphology, atomic and electronic structure both SiO_2CuOx and $SiO_2(CuO_xSnO_y)$ films synthesized at the same amount Cu and addition Sn into the sol, to elucidate chemical state and the nature chemical bonding of Cu and Sn at surface and in volume of films during the formation of

http://dx.doi.org/10.1016/j.apsusc.2016.02.245
0169-4332/

samples and preliminary to estimate they influence on sensitivity to NO_2.

2. Materials and experimental methods

2.1. Films preparation

A sol for fabrication of the SiO_2CuO_x thin film was prepared from the alcoholic solutions on the basis of tetraethoxysisilane with the addition of $Cu(NO_3)_2$ in an Cu amount of 5 wt.% [25]. Sol of the Cu/Sn precursor was obtained by the adding of $SnCl_4$ in an amount of 3 wt.% of Sn to previous solution. The precursors were deposited on to oxidized silicon substrates by spin coating technique in seven days after preparation. The films prepared by the technique as the result of this procedure were first dried at 150 °C for 2 h and then annealed at 500 °C for 5 h in air. Thickness of the annealed films was estimated by an elipsometry and SEM methods to be ~0.2 μm at the bottom of the porous and ~1.5 μm as whole layer for the spin coater rotating speed of 3000 rpm for 30 s.

2.2. Films characterization

Surface morphological study of the deposited film samples was carried out using a scanning electron microscopy (LEO 1560, ZEISS) with operating voltage at 5 kV. Silicon substrate, coating interface and location of crystallites was studied from the cross sectional samples. The chemical analysis of the films was investigated using an energy dispersive X-ray (EDX) analyzer (Oxford Instruments). All measurements were carried out using complex analytic device based on scanning electron microscope VEGA II LMU with operating voltage at 20 kV and system of the microanalysis INCA ENERGY 450/XT with X-Act DDD detector. The statistical parameters of the surface morphology, namely the mean-average roughness, were estimated using Image Analysis software [26].

X-ray diffraction (XRD) phase analysis was performed with an ARL X'TRA diffractometer, the X-ray source used Cu Kα radiation (λ = 1.5418 Å). All scans were made in the grazing incidence mode, with incidence angles ω of 2 or 3°.

Complementary, the bonding structure with element sensitivity to Cu, Sn and O as well as the local environment of Cu ions was studied by the XPS (X-ray photoelectron spectroscopy), NEXAFS (Near edge X-ray absorption fine structure) and XANES (X-ray absorption near edge structure) spectroscopies using soft X-rays at the Russian-German Laboratory (RGL) and hard X-rays at the beamline KMC-2 of BESSY II synchrotron radiation facility (Germany, Berlin). The XPS spectra of SiO_2CuO_x and $SiO_2(CuO_xSnO_y)$ films were measured in the normal photoemission registration mode by using the Phoibos 150 spherical analyzer from Specs at the energy of monochromatized synchrotron radiation equals to 1030 eV, with energy resolution of 0.2 eV and probing depth of a ~5 Å. Deconvolution of the Cu $2p_{3/2}$, Sn $3d_{5/2}$, O 1s XPS peaks was performed with XPSPEAK software, using the Gaussian/Lorenzian sum function and a Shirley base line as the background for each peak.

Cu L-edge NEXAFS spectra with photon energy resolution at 0.1 eV were recorded in the total electron yield detection mode (TEY) measuring the photocurrent emitted from the specimen surface with a typical probing depth of ~50 Å. The samples were located at the angle of 45° with respect to the incident beam of monochromatic radiation. The size of the focused spot on the sample was ~0.1 × 0.1 mm^2. The Cu K-edge XANES spectra were measured in fluorescence mode using double-crystal $Si_{1-x}Ge_x$ (1 1 1) monochromator. Pre-edge features were collected using 0.3 eV steps whereas the main edge jump was collected with 0.7 eV till 240 eV above the absorption edge. Samples were set up at grazing incidence geometry (~5° to the incident X-ray beam) in order to enhance the detection efficiency.

2.3. Gas sensitive property test

The electrical and gas sensitivity tests were carried out in the calibration test bench equipped with a heating element [27]. The calibration test bench included a gas chamber (V = 1 dm^3), a data-collection system RL-88AC (an analog-digital, digital-analog converter with the RealLab software). The sensor element was set on the heater inside the gas chamber. The RL-88AC data-collection system controlled the resistance by a resistance-voltage converter. The gas-sensitive characteristics of the films were tested to NO_2 inputs. The magnitude of the response was defined as the change in resistance of the sample on exposure to gas. The gas sensing response (S) was calculated with the formula [28]: $S = (Ra - Rg)/Rg$, where Ra is the resistance of the sensing element in air, Rg is the resistance of the sensing element in a given target gas.

3. Results and discussion

3.1. Morphology, structure and composition

SEM technique was used to examine the surface of the films (Fig. 1) and the analyses indicated that there were large differences in microstructure between both types of samples. The surface of the SiO_2CuO_x film has evenly porous structure (Fig. 1a), formed by a silica matrix with pores of average diameter ~8 μm. Formation of the copper oxide flower-like agglomerates are clearly visible both on the surface of the silica matrix (see example in inset of Fig. 1a) and embedded within pores (Fig. 1c). As one can see the agglomerates have spherical shape flower-like structure with diameter in the range of 0.7–1.0 μm composed of many interconnected copper oxides crystallites with the size of 30–50 nm (Fig. 1b). Such flower-like agglomerates increase the total surface area of the films and play role of the adsorption centers.

Fig. 1(d–f) demonstrate the effect of addition small amount (3 wt.%) of Sn into cooper-containing sol, that results in changing of surface morphology of films as well as shape and size of crystallites. The silica matrix of tin-containing films $SiO_2(CuO_xSnO_y)$ has smooth, more densified morphology with pores in the range of 1.0–12 μm (Fig. 1d). The films reveal a large number well separated grains, with sizes in the range of 150–500 nm (Fig. 1d inset, e). Formed crystallites mainly accumulated inside of the pores (Fig. 1d). As one can see on Fig. 1f on the bottom of pores there are, supposedly, copper-containing structures (dark-grey color) and SnO_y particles (light-grey color). Also, the SEM images of the cross-section SiO_2CuO_x and $SiO_2(CuO_xSnO_y)$ shows interfaces of the films: composite layer/SiO_2/Si substrate. The thickness of the composite layer can be estimated as ~0.2–1.5 μm (inside the pores and a full layer, respectively). Structure of the SiO_2 and Si substrate appears to be flat and featureless, while there is an impure structure for composite layers.

Both samples were analyzed by X-ray diffraction to determine the presence of copper and tin crystallized phases. It should be remarked that a multiphase system is present in both samples. As shown Fig. 1c (inset) for case of SiO_2CuO_x film, the diffraction peaks at θ = 25.1°, 31.18° can be indexed to the SiO_2 phase, at θ = 34.61°, 34.84° are attributed to the typical Cu_2O phase, the diffraction peaks at θ = 41.77°, 45.78°, 51.80° are assigned to the CuO and at θ = 25.67°, 27.91° to the $CuSiO_3$. This result is in good agreement with the other XRD reports [29,30]. In the case of $SiO_2(CuO_xSnO_y)$ films, apart from diffraction peaks corresponding to the SiO_2CuO_x films, there are new diffraction peaks appear at θ = 26.57°, 33.32° and 51.59°, corresponding to the SnO_2, indicating the presence of

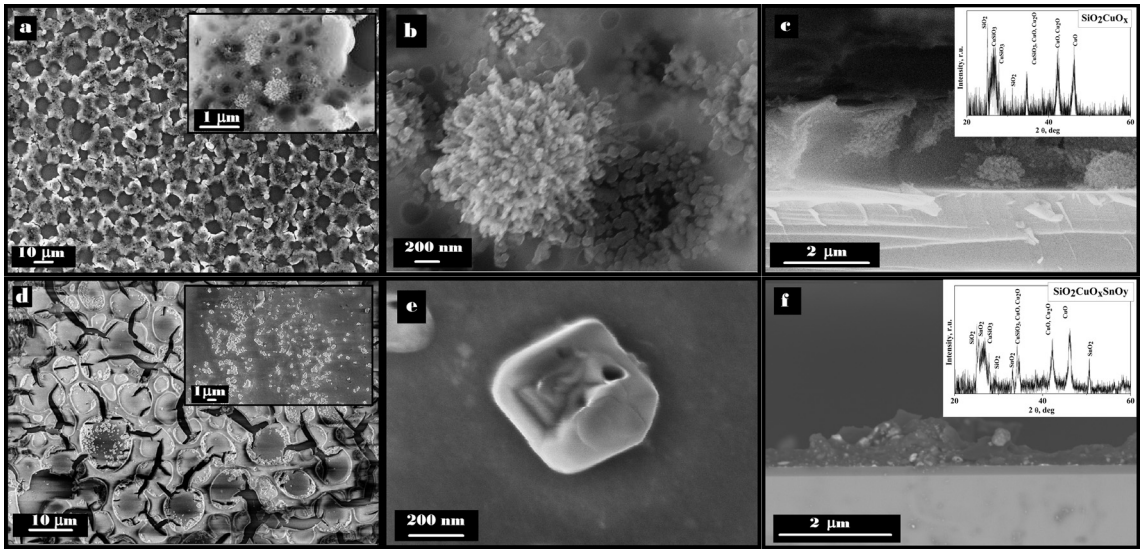

Fig. 1. SEM images of the surface morphology of the SiO_2CuO_x film: (a) scale 10 μm (inset 1 μm), (b) 200 nm, (c) cross section (2 μm) and XRD pattern (inset); $SiO_2(CuO_xSnO_y)$ film: (d) scale 10 μm (inset 1 μm), (e) 200 nm, (f) cross section (2 μm) and XRD pattern (inset).

this phase in the sample. This observation indicates that the crystal structure of copper oxides is intact with the addition of tin. Adding Sn does not lead to the formation of a new mixed phase (diffraction pattern peaks appear at specific degrees for separate phases of copper CuO, Cu_2O, $CuSiO_3$ and SnO_2). The relatively broader diffraction peaks suggests that the smaller crystallite size nucleus. It is in agreement with SEM data, which indicates that copper oxide agglomerates includes small crystallites with the size of 30–50 nm. Besides, we assume that small copper oxides nanoparticles and copper ions embedded in a silicon matrix, as evidenced by the data of XPS and XANES presented below. With addition of tin the diffraction peaks of CuOx phase are weaker, that in accordance of Ref. [31] can be ascribed to well dispersed small CuOx nanoparticles on the surface of SnO_2.

SEM-EDX study was carried out to clarify chemical composition in different points of $SiO_2(CuO_xSnO_y)$ film, namely: silica matrix (point 1), particles inside of pores (point 2) and bottom of the pore (point 3). In Fig. 2 the image of surface $SiO_2(CuO_xSnO_y)$ film under SEM and corresponding EDX point analysis is shown. Note that the minimum electron beam spot size achievable for the EDX analysis was approximately 500 nm, that allows estimate Cu/Sn ratio rather accurate. The results indicate that the average wt.% ratio of Cu/Sn is about 18.81/10.73 for this sample.

3.2. XPS investigations

In order to investigate the chemical species formed as result of addition of the Sn to copper containing solution XPS profiles were obtained by scanning the Cu 2p, Sn 3d and O 1s regions. The Cu $2p_{3/2}$ and Sn $3d_{5/2}$ peaks are relatively broad and seem to be influenced by the presence of mixed copper and tin species. This is in agreement with the XRD data, where pattern of the samples contains broad peaks which characterize different states of copper and tin. In addition, energy shift and breadth of the O 1s peaks for SiO_2CuO_x and $SiO_2(CuO_xSnO_y)$ displays that these atoms must lie in different chemical environments. The shape analysis of corresponding XPS $Cu2p_{3/2}$, $Sn3d_{5/2}$ and O1s peaks using the decomposition procedure with Gaussian mixed function was performed (Fig. 3). Decomposition of Cu $2p_{3/2}$ peak of the SiO_2CuOx and $SiO_2(CuO_xSnO_y)$ films is depicted in Fig. 3a and b respectively. The summarize binding energy (BE) and relative peak areal intensity of main components of XPS $Cu2p_{3/2}$, $Sn3d_{5/2}$, O1s peaks of

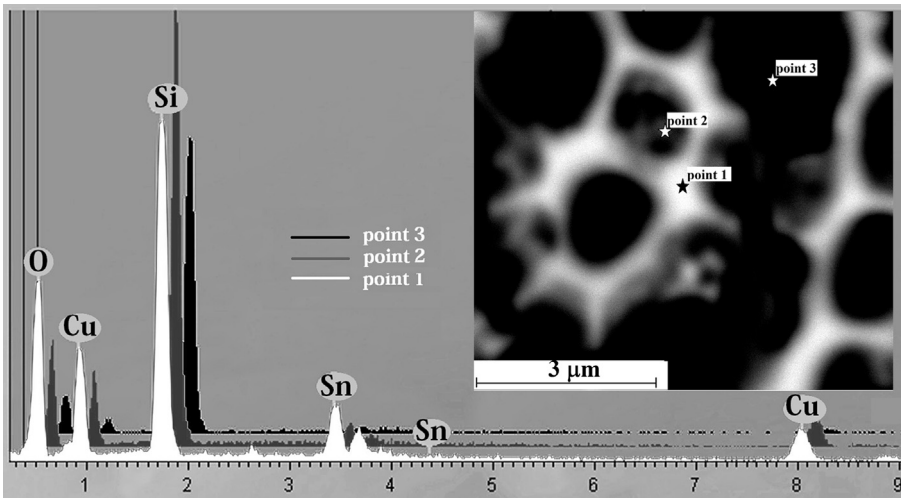

Fig. 2. EDX point analysis of a selected area (inset) $SiO_2(CuO_xSnO_y)$ film: silica matrix (point 1), particles inside of pores (point 2) and bottom of the pore (point 3).

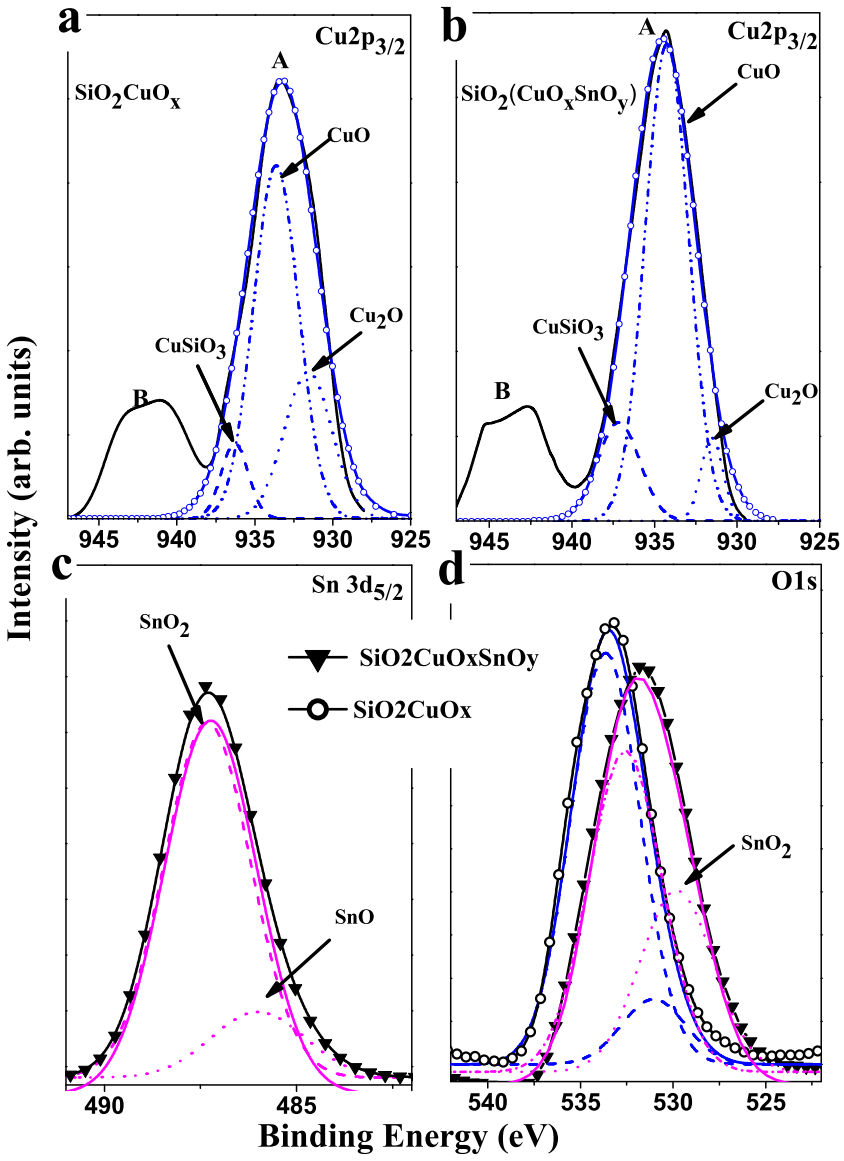

Fig. 3. Decomposition of main components of XPS Cu2$p_{3/2}$, Sn3$d_{5/2}$, O1s peaks of SiO_2CuO_x and $SiO_2(CuO_xSnO_y)$ films: (a) and (b) decomposition the Cu $2p_{3/2}$ of SiO_2CuO_x and $SiO_2(CuO_xSnO_y)$ respectively (dot line—Cu_2O, dash line—$CuSiO_3$, dash dot line—CuO, solid line—fit); (c) Sn $3d_{5/2}$ (dot line—SnO, dush line—SnO_2, solid line—fit; (d) O 1s (dot line—SnO_2).

Table 1
The binding energy (BE) and relative peak areal intensity (S) of main components of XPS Cu2$p_{3/2}$, O1s and Sn3$d_{5/2}$ peaks of SiO_2CuO_x and $SiO_2(CuO_xSnO_y)$.

Sample	Cu $2p_{3/2}$		O 1s		Sn $3d_{5/2}$	
	BE, eV	S	BE, eV	S	BE, eV	S
SiO_2CuO_x	931.6	668	531.6	1638		
	933.7	1528	533.6	11168		
	935.0	196				
$SiO_2(CuO_xSnO_y)$	931.7	164	529.8	5247	487.0	361
	934.2	1856	532.6	9167	486.0	1798
	937.3	374				

SiO_2CuO_x and $SiO_2(CuO_xSnO_y)$ are presented in Table 1. In accordance to referenced data, the observation of obvious shake-up peaks (B) in both samples can be attributed to the Cu^{2+} oxidation state [32], but absence of clear peak B splitting indicates an availability of the mixed oxidation Cu state [33]. The broadened Cu $2p_{3/2}$ peaks were correspondingly decomposed into three distinct peaks. The lower energy peaks being associated with Cu_2O. The peaks with maximal intensity correspond to the CuO. The peaks with higher energy can be attributed to divalent copper compounds such as $Cu(OH)_2$ or $CuSiO_3$. To summarize all these facts, the result indicates that the oxidation state of Cu was heterogeneous with mixing of Cu^{2+} and Cu^{+} states, namely: divalent copper oxide CuO, with a mixture of monovalent oxide Cu_2O and divalent double oxide $CuSiO_3$ and/or hydroxide $Cu(OH)_2$ [34]. The Cu 2p binding energies of $Cu(OH)_2$ and $CuSiO_3$ are almost indistinguishable by XPS because the binding energies are superimposed. Probability of $Cu(OH)_2$ formation is small. The $Cu(OH)_2$ decomposes at the temperatures of 50–60 °C. The CuO and Cu_2O oxides formed after the thermal treatment of the films at 500 °C are stable for chemical transformations to $Cu(OH)_2$ phase. The processes of Cu-Si bonding begin in the sol. The adding of Sn prevents decomposition of this bond and $CuSiO_3$ is formed in the film after thermal treatment. As one can see from spectral analysis, the relative content of Cu component is differ for SiO_2CuO_x and $SiO_2(CuO_xSnO_y)$ films. The

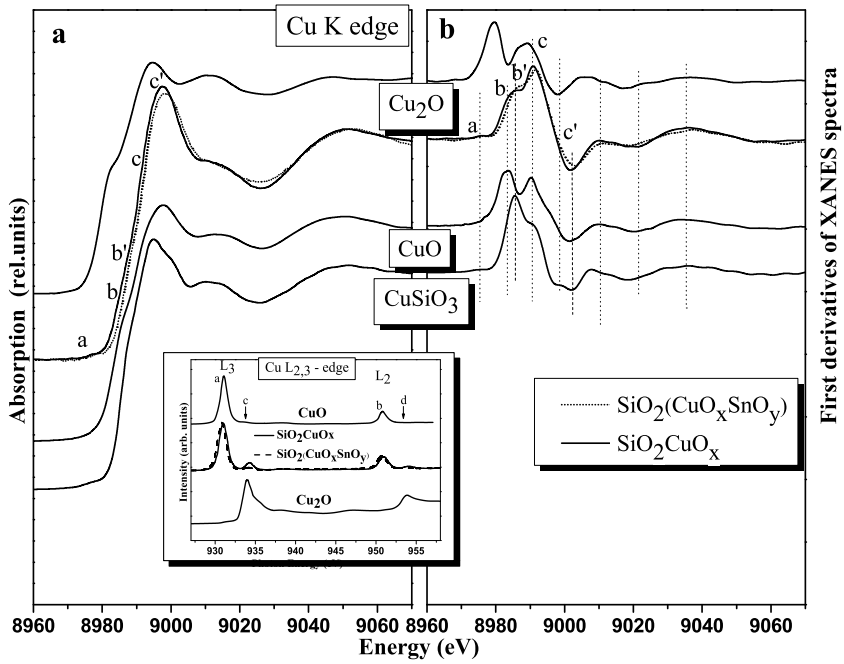

Fig. 4. Normalized Cu K-edge XANES spectra of SiO_2CuO_x and $SiO_2CuO_xSnO_y$ films compared with a reference compounds CuO (formally Cu^{2+}), Cu_2O (formally Cu^+) and natural mineral of black dioptase $CuSiO_3$ (formally Cu^{2+}) (a); first derivatives of the corresponding XANES spectra (b); inset —Cu $L_{2,3}$-edge NEXAFS spectra of SiO_2CuO_x and $SiO_2CuO_xSnO_y$ films compared with a reference compounds: CuO (formally Cu^{2+}), Cu_2O (formally Cu^+).

contribution of Cu_2O decreasing with simultaneous increasing of Cu^{2+} for $SiO_2(CuO_xSnO_y)$ film. As shown in Fig. 3c, the weak peak at 486.0 eV and dominant peak at 487.2 eV for the XPS binding energy of tin were observed. The Sn $3d_{5/2}$ core peak at 487.2 eV may be assigned to Sn(IV) [34,35]. The low binding energy (BE ~ 486 eV) may be characteristic monoxide tin coated by the SnO_2 [36]. Majid et al. [37] have reported that the Cu 2p peaks for SnO_2:CuO samples shift by 0.4 eV towards higher energies from its value for CuO. It was observed for CuO components in $SiO_2(CuO_xSnO_y)$. Similarly, the core level O 1s spectra of both samples are displayed in Fig. 3d. A large value FWHM (full width at half maximum) of both films suggests that the XPS line is formed by the electrons of various oxides of copper, silicon and tin. As one can see, adding tin in the sample leads to a shift of the oxygen species toward lower energies (an oxide with a greater degree of oxidation), reduction in the intensity and increase the parameter FWHM from 4.1 to 4.6 eV. The decomposition of O 1s core peak of both samples shows two main components: with large intensity at high binding energy and more small intensity at low binding energy. The binding energy of the O1s-levels for different structural and surface modifications of silicon oxide SiO_2 may vary from 532.1 eV up to 533.7 eV, respectively [38]. Also, the high binding energies component with maximum at 532.5–533.7 eV, having the large value of FWHM can be associated with copper/silicon oxide mixture (531.7 eV) [39], as well as dioxide SnO_2 (530.0–531.2 eV), Cu—O binding energy and oxygen atoms chemisorbed at the surface, that is in a good agreement with the Yea et al. [40], who have proposed the energetic position of this component close to 533.0 eV. A more precise analysis is not possible due to large value FWHM and more number of superimposed peaks.

3.3. XAS study

The XAS (NEXAFS and XANES) spectroscopy has been applied to understand the differences in oxidation states and local surrounding of Cu ions for both SiO_2CuO_x and $SiO_2(CuO_xSnO_y)$ films. In Fig. 4 (inset) the Cu $L_{2,3}$ NEXAFS spectra of both samples in comparison with referenced compounds are shown. For both samples L_3 and L_2 resonance peaks are symmetric and display the fine structure, namely divide into two clear features “a”, “c” and “b”, “d” respectively. The appearance of a shoulder peaks (c, d) above the $L_{2,3}$-edges suggests the existence of a small amount of Cu^{1+} ions, while most of the Cu ions are divalent as indicated by the large peaks “a” and “b” in the spectra of both films under studying. The spectral features in the Cu L_3-edge area were analyzed to quantitatively determine the valence of copper in the both samples. The two peaks at ~931.0 eV (due to Cu^{2+}) and ~934.0 eV (due to Cu^{1+}) were fitted with Gaussian functions after approximating the background with a straight line (Table 2). The Cu $L_{2,3}$-edge NEXAFS study has provided evidence for addition of Sn to sol: seen were both the reduction of an additional absorption peak due to nominally monovalent copper and simultaneous increasing in the intensity of the peak due to nominally divalent copper. That is suggesting decreasing of Cu_2O in layers up ~50 Å, which are working layers of gas sensors. To investigate deeper layers Cu K-edge XANES spectra of both samples, referenced compounds and its first derivative was analyzed (Fig. 4a and b respectively). It was found that the energy position and shape XANES features of as-synthesized samples are closer to that of CuO and $CuSiO_3$, rather than those of Cu_2O. But, the differences in the energy range 8970–9002 eV are observed between samples under study and CuO as well as $CuSiO_3$. In accordance with derivatives it is clear that peak “b” corresponds to $CuSiO_3$ while peak “c” mainly to CuO. Besides, weak pre-edge peak “a” is observed in $CuSiO_3$ only. All this clear reflects existence of linear combination of signals from Cu atoms with neighborhood similar to that found in CuO and in

Table 2
Characterization results of fitting Cu L_3-edge XANES spectra with Gaussian functions for the SiO_2CuO_x and $SiO_2CuO_xSnO_y$ films: energy positions (E) and the fitted peak areal intensities (I) corresponding to (Cu^{2+}) and (Cu^+).

Sample	E (eV) peak “a”	I [Cu^{2+}] peak “a”	E (eV) peak “c”	I [Cu^+] peak “c”
SiO_2CuO_X	931.1	1.27	934.4	0.2
$SiO_2(CuO_xSnO_y)$	930.8	1.3	933.9	0.1

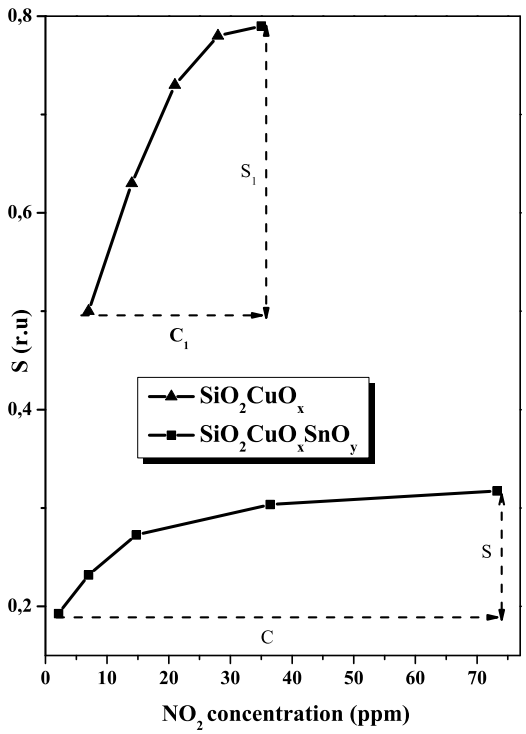

Fig. 5. Gas sensor response to NO_2 gas for $SiO_2SnO_xCuO_y$ and SiO_2CuO_x films at the concentrations range of 1–70 ppm in air at 170 °C. The C_1, C and S_1, S arrows shows differences in concentration range and sensor response for SiO_2CuO_x and $SiO_2(CuO_xSnO_y)$ films.

$CuSiO_3$. Also, energy peak shift "b" to position "b′", redistribution of intensity "b" and "c" peaks, appearance of "c′" shoulder at the $SiO_2CuO_xSnO_y$ spectrum in comparison with SiO_2CuO_x film can be associated with increasing of $CuSiO_3$ after addition of Sn. The results suggest that CuO and $CuSiO_3$ formed in all volume of samples, not only at surface.

3.4. Gas sensitivity to NO_2

Gas sensitivity of the SiO_2CuOx and $SiO_2(CuO_xSnO_y)$ was tested to NO_2 inputs to be varied in the concentrations range of 1–70 ppm in air at 170 °C. Fig. 5 shows correlation between the phase composition and gas sensitive characteristics of the films. As it turned out, the concentration range of NO_2 gas which could be detected by the sensors is 1–70 and 7–25 ppm for $SiO_2CuO_xSnO_y$ and SiO_2CuO_x respectively. Thus, the addition of tin allows to extend the range of detectable concentrations. But, gas sensitivity tests showed that the sensor response (S) to NO_2 gas of SiO_2CuO_x film is greater than the response of $SiO_2CuO_xSnO_y$ one.

In our case, role of the tin is to provide gas sensitivity of the film and the role of the copper is to provide slectivity to NO_2 molecules. That is why the best way to improve gas sensitive is to find out such Sn/Cu ratio wich would provide fast and high response to wide concentration range and also good selectivity to NO_2 gas.

4. Conclusions

Sol-gel method was applied to the preparation of SiO_2CuO_x and $SiO_2(CuO_xSnO_y)$ films. SEM shows that the addition of $SnCl_4$ in sol affects on surface morphology and shape of crystallites synthesized films. The transition from flower-like copper oxide agglomerates (700–900 nm) of spherical shape in SiO_2CuO_x films to grains (150–500 nm) in $SiO_2(CuO_xSnO_y)$ films is observed. So, the tin adding prevents the formation of the flower-like agglomerates. The average wt.% ratio of Cu/Sn is about 18.81/10.73. The main phase of copper for both films is CuO with lower amount of Cu_2O and $CuSiO_3$. The amount of Cu_2O phase decreases, while CuO and $CuSiO_3$ phase increases with addition tin both on the surface and in deeper layers of the samples. According to SEM, EDX, XPS studies we assume that mixed-oxide crystallites are formed and $SiO_2(CuO_xSnO_y)$ grains consist of copper-containing oxides and SnO_2. Presence of tin oxide particles in the films decreases the response to NO_2 gas, but at the same time expands the range of detectable concentrations. So, the effect of mixing copper and tin oxides in the silicon matrix to the gas sensor response is nonunique and requests further investigation.

Acknowledgements

This work was supported by the Ministry of education and science of the Russian Federation (grant no. 11.2432.2014/K). We thank HZB (Berlin, Germany) for the allocation of synchrotron radiation beamtime (RGBL and KMC-2 at BESSY II), The authors wish to thank Prof. A. T. Kozakov for valuable discussion.

References

[1] M. Yang, J. He, J. Colloid Interface Sci. 144 (2012) 229.
[2] S. Singh, B.C. Yadava, R. Prakash, B. Bajaj, J. Rocklee, Appl. Surf. Sci. 257 (2011) 10763.
[3] Z.Q. Yu, C.M. Wang, M.H. Engelhard, P. Nachimuthu, D.E. Mc Cready, I.V. Lyubinetsky, S. Thevuthasan, Nanotechnology 18 (2007) 115601.
[4] O. Akhavan, H. Tohidi, A.Z. Moshfegh, Thin Solid Films 517 (2009) 6700.
[5] R.C. Beatriz, B. Farzad, Surf. Sci. Rep. 70 (2015) 135.
[6] G. Korotcenkov, B.K. Cho, Sens. Actuators B 161 (2012) 28.
[7] B. Afzal, N. Cioffi, L. Sabbatini, L. Torsi, Sens. Actuators B 171–172 (2012) 25.
[8] G. Biasotto, M.G.A. Ranieri, C.R. Foschini, A.Z. Simoes, E. Longo, M.A. Zaghete, Ceram. Int. 40 (2014) 14991.
[9] J. Sharma, N.K. Chaki, A.B. Mandale, R. Pasricha, K. Vijayamohanan, J. Colloid Interface Sci. 272 (2004) 145.
[10] B. Liu, H.C. Zeng, J. Am. Chem. Soc. 126 (2004) 8124.
[11] X.M. Lin, A.C.S. Samia, J. Magn. Magn. Mater. 305 (2006) 100.
[12] C.H. Kuo, C.H. Chen, M.H. Huang, Adv. Funct. Mater. 17 (2007) 3773.
[13] X. Zhang, Z. Cui, Mater. Sci. Eng. B 162 (2009) 82.
[14] L. Li, C. Nan, Q. Peng, Y. Li, Chem. Eur. J. 18 (2012) 10491.
[15] Y. Mao, J. Hea, X. Sun, W. Li, X. Lu, J. Gana, Z. Liu, L. Gong, J. Chen, P. Liu, Y. Tong, Electrochim. Acta 62 (2012) 1.
[16] M. Vaseem, A. Umar, Y.B. Hahn, D.H. Kim, K.S. Lee, J.S. Jang, J.S. Lee, Catal. Commun. 10 (2008) 11.
[17] E. Mohammadi-Manesh, M. Vaezzadeh, M. Saeidi, Comput. Mater. Sci. 97 (2015) 181.
[18] A. Klinbumrung, T. Thongtem, S. Thongtem, Appl. Surf. Sci. 313 (2014) 640.
[19] J. Jiang, Y.Y. Li, J.P. Liu, X.T. Huang, C.Z. Yuan, X.W. Lou, Adv. Mater. 24 (2012) 5166.
[20] A. Banerjee, M. Dutta, S. Bysakh, A.K. Bhowmick, T. Laha, Appl. Surf. Sci. 313 (2014) 804.
[21] D. Tiwari, T.K. Chaudhuri, T. Shripathi, U. Deshpande, J. Phys. Chem. Solids 75 (2014) 410.
[22] G. Battaglin, E. Cattaruzza, F. Gonella, R. Polloni, B.F. Scremin, G. Mattei, P. Mazzoldi, C. Sada, Appl. Surf. Sci. 226 (2004) 52.
[23] B. Balamurugan, B.R. Mehta, S.M. Shivaprasad, Appl. Phys. Lett. 79 (2001) 3176.
[24] V.A. Shmatko, G.E. Yalovega, T.N. Myasoedova, M.M. Brzhezinskayac, I.E. Shtekhin, V.V. Petrov, Phys. Solid State 57 (2) (2015) 399.
[25] N.K. Plugotarenco, A.N. Korolev, V.V. Petrov, T.N. Nazarova, Inorg. Mater. 43 (2007) 1010.
[26] Image Analysis software http://www.ntmdt.com/.
[27] V.V. Petrov, T.N. Nazarova, A.N. Korolev, N.F. Kopylova, Sens. Actuators B. 133 (2008) 291–295.
[28] L.A. Patil, D.R. Patil, Sens. Actuators B 120 (2006) 316–323.
[29] Z.H. Liang, Y.J. Zhu, Chem. Lett. 34 (2005) 214–215.
[30] W.W. Wang, Y.J. Zhua, G.F. Cheng, Y.H. Huang, Mater. Lett. 60 (2006) 609–612.
[31] H. Mai, D. Zhang, L. Shi, T. Yan, H. Li Appl, Surf. Sci. 257 (2011) 7551–7559.
[32] J. Morales, A. Caballero, J.P. Holgado, J.P. Espinós, A.R. González-Elipe, J. Phys. Chem. B 106 (2002) 10185.
[33] J. Park, K. Lim, R.D. Ramsier, Y.C. Kang, Bull. Korean Chem. Soc. 32 (9) (2011) 3395.
[34] NIST X-ray Photoelectron Spectroscopy Database http://srdata.nist.gov/xps/Default.aspx.
[35] P.H. Watts, J.E. Huheey, Inorg. Nucl. Chem. Lett. 10 (4) (1974) 287.
[36] O.A. Chuvenkova, E.P. Domashevskaya, S.V. Ryabtsev, Y.A. Yurakov, A.E. Popov, D.A. Koyuda, D.N. Nesterov, D.E. Spirin, R.Y. Ovsyannikov, S.Y. Turishchev, Phys. Solid State 57 (1) (2015) 153–161.

[37] Abdul Majid, James Tunney, Steve Argue, David Kingston, Michael Post, James Margeson, Graeme J. Gardner, J. Sol Gel Sci. Technol. 53 (2) (2010) 390–398.
[38] V.I. Nefedov, X-ray photoelectron spectroscopy of chemical compounds, Moscow: Chem. (1984).
[39] R.P. Netterfield, P.J. Martin, C.G. Pacey, W.G. Sainty, D.R. McKenzie, J. Appl. Phys. 66 (1989) 1805–1809.
[40] B. Yea, H. Sasaki, T. Osaki, K. Sughara, R. Konishi, J. Appl. Phys. 38 (1999) 2103.

G.E. Yalovega*
Faculty of Physics, Southern Federal University, Zorge Str. 5, Rostov-on-Don 344090, Russia

T.N. Myasoedova
Institute of Management in Economic, Ecological and Social Systems, Southern Federal University, Chekhov str. 2, Taganrog 347928, Russia

V.A. Shmatko
Faculty of Physics, Southern Federal University, Zorge Str. 5, Rostov-on-Don 344090, Russia

M.M. Brzhezinskaya
Helmholtz Zentrum Berlin fur Materialien und Energie, Albert Einstein Str. 15, Berlin 12489, Germany

Yu. V. Popov
Institute of Earth sciences, Southern Federal University, Zorge str. 40, Rostov-on-Don 344090, Russia

* Corresponding author.
E-mail address: yalovega1968@mail.ru
(G.E. Yalovega)

8 September 2015

20 February 2016

27 February 2016
Available online 2 March 2016